

Divergent modes for cargo-mediated control of clathrin-coated pit dynamics

Amanda L. Soohoo and Manojkumar A. Puthenveedu

Department of Biological Sciences, Carnegie Mellon University, Pittsburgh, PA 15213

ABSTRACT Clathrin-mediated endocytosis has long been viewed as a process driven by core endocytic proteins, with internalized cargo proteins being passive. In contrast, an emerging view suggests that signaling receptor cargo may actively control its fate by regulating the dynamics of clathrin-coated pits (CCPs) that mediate their internalization. Despite its physiological implications, very little is known about such “cargo-mediated regulation” of CCPs by signaling receptors. Here, using multicolor total internal reflection fluorescence microscopy imaging and quantitative analysis in live cells, we show that the μ -opioid receptor, a physiologically relevant G protein-coupled signaling receptor, delays the dynamics of CCPs in which it is localized. This delay is mediated by the interactions of two critical leucines on the receptor cytoplasmic tail. Unlike the previously known mechanism of cargo-mediated regulation, these residues regulate the lifetimes of dynamin, a key component of CCP scission. These results identify a novel means for selectively controlling the endocytosis of distinct cargo that share common trafficking components and indicate that CCP regulation by signaling receptors can operate via divergent modes.

Monitoring Editor

David G. Drubin
University of California,
Berkeley

Received: Jul 26, 2012

Revised: Mar 19, 2013

Accepted: Mar 21, 2013

INTRODUCTION

Clathrin-mediated endocytosis (CME), the main mode by which cells internalize surface cargo proteins, including physiologically relevant signaling receptors, is a highly ordered process mediated by sets of core endocytic proteins (Kaksonen *et al.*, 2000; McMahon and Boucrot, 2011; Taylor *et al.*, 2011; Boettner *et al.*, 2012; Rao *et al.*, 2012). CME is initiated by endocytic cargo and membrane-remodeling proteins that recruit adapter proteins, such as AP2 and β -arrestin,

and clathrin to the plasma membrane (Santini *et al.*, 1998; Wolfe and Trejo, 2007; Kelly and Owen, 2011; McMahon and Boucrot, 2011). The growing clathrin-coated pit (CCP) is then stabilized by the interactions of adapter proteins with cargo (Santini *et al.*, 1998; Ehrlich *et al.*, 2004). Recent studies following fluorescently tagged components of the clathrin endocytic machinery described a modular arrangement for the recruitment of proteins during CME, with relatively distinct sets of proteins acting during initiation, maturation, completion, and scission phases of vesicle formation during endocytosis (Kaksonen *et al.*, 2000; Taylor *et al.*, 2011).

The traditional view of CME was that it was controlled entirely by a cascade of interactions of core endocytic proteins, with regulation being mainly at the level of cargo-adapter interactions. This view has been challenged by evidence that signaling receptor cargo can regulate the dynamics of the CCPs to which they localize (Puthenveedu and von Zastrow, 2006; Henry *et al.*, 2012). This is particularly interesting because the internalization of signaling receptors has several direct physiological consequences to their signaling (Marchese *et al.*, 2008; Sorkin and von Zastrow, 2009; Magalhaes *et al.*, 2012). The only known examples for signaling cargo that regulate CCPs are the β -adrenergic receptors—prototypical members of the G protein-coupled receptor (GPCR) family, the largest family of signaling receptors (Pierce *et al.*, 2002). Adrenergic receptors localize to a distinct subset of CCPs and selectively delay the dynamics of those CCPs (Puthenveedu and von Zastrow, 2006). This delay is mediated by interactions of the receptor C-terminal tail

This article was published online ahead of print in MBoc in Press (<http://www.molbiolcell.org/cgi/doi/10.1091/mbc.E12-07-0550>) on March 27, 2013.

Address correspondence to: Manojkumar A. Puthenveedu (map3@andrew.cmu.edu).

Abbreviations used: AP2, adapter protein 2; B2AR, β 2-adrenergic receptor; B2HA, B2AR with C-terminal HA-tag; CALM, clathrin assembly lymphoid myeloid leukemia protein; CME, clathrin-mediated endocytosis; CPPs, clathrin-coated pits; DADLE, D-Ala², D-Leu⁵-enkephalin; DAMGO, D-Ala², N-Me-Phe⁴, Gly⁵-ol-enkephalin; DOR, δ -opioid receptor; FLAG, DYKDDDDK peptide; GPCR, G-protein-coupled receptor; MOR, μ -opioid receptor; MOR-LLAA, MOR with LENLEAE mutated to AENAEAE; NECAP, adaptin ear-binding clathrin-associated protein; PDZ, postsynaptic density protein/Drosophila disc large tumor suppressor/zonula occludens-1 protein; SpH, pH-sensitive green fluorescent protein; TIRFM, total internal reflection fluorescence microscopy; TTP, transferrin receptor trafficking protein.

© 2013 Soohoo and Puthenveedu. This article is distributed by The American Society for Cell Biology under license from the author(s). Two months after publication it is available to the public under an Attribution-Noncommercial-Share Alike 3.0 Unported Creative Commons License (<http://creativecommons.org/licenses/by-nc-sa/3.0>).

“ASCB,” “The American Society for Cell Biology,” and “Molecular Biology of the Cell” are registered trademarks of The American Society of Cell Biology.

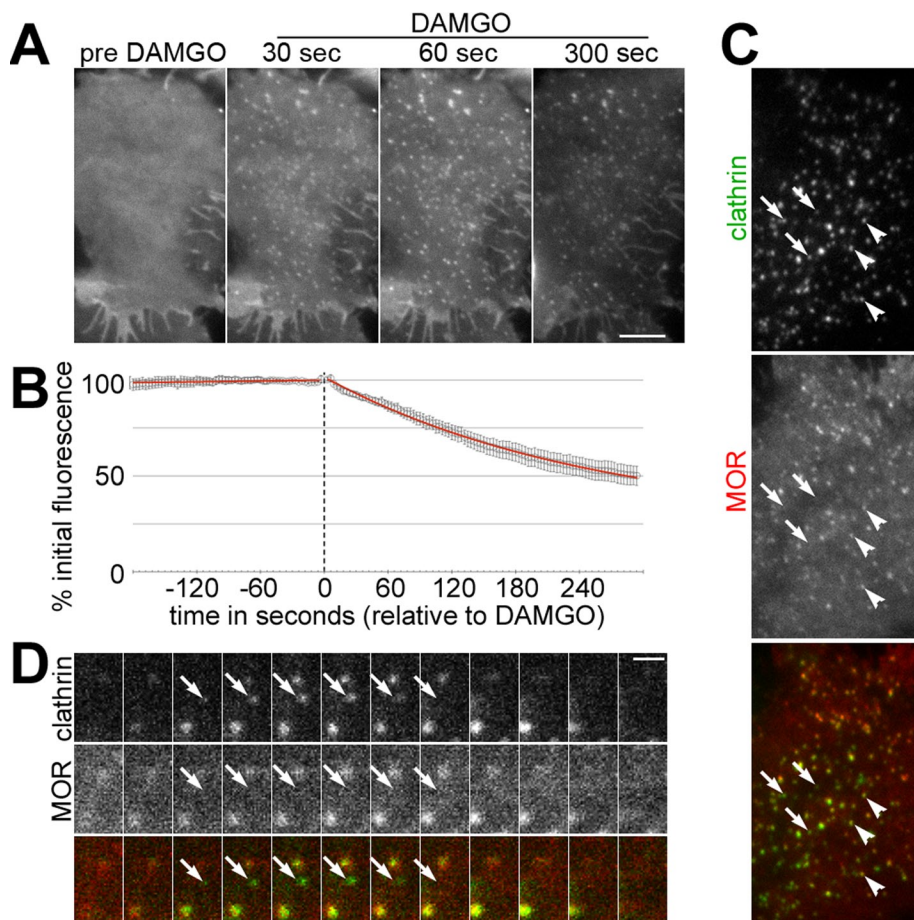


FIGURE 1: MOR internalizes via a subset of clathrin-coated pits. (A) Representative images from an example cell expressing SpH-tagged MOR imaged by TIRFM before and 30, 60, and 300 s after activation by the MOR agonist DAMGO, showing rapid MOR clustering. Scale bar, 5 μ m. (B) Average surface fluorescence values over time, \pm SEM, from multiple cells, from 3 min before to 5 min after DAMGO, showing an exponential decrease after DAMGO. Red line shows curve fit to linear (before) or single-phase decay (after). (C) Dual-color TIRFM of MOR (red) and clathrin (green), showing clustering of MOR in a subset of coated pits (arrowheads). Arrows indicate example CCPs without detectable MOR. Scale bar, 5 μ m. (D) Frames from a dual-color TIRFM time series 3 s apart, showing the complete cycle of an example CCP (arrows), from formation to internalization, without detectable MOR fluorescence. MOR is in red and clathrin in green. Two example CCPs that show MOR clustering are also shown. Scale bar, 1 μ m.

with the actin cytoskeleton, which delay the recruitment, but not the activity, of the GTPase dynamin—a key member of the scission module (Schmid and Frolov, 2011; Ferguson and De Camilli, 2012). The fact that β -2 adrenergic receptor (B2AR) can control CCPs opens the possibility that cells can exert virtually unlimited selective control over the endocytosis of diverse cargo using shared trafficking components.

The μ -opioid receptor (MOR) is a related and clinically relevant signaling GPCR that is internalized via CCPs (Keith *et al.*, 1996; Segredo *et al.*, 1997). MOR mediates the physiological effects of endogenous opioid neurotransmitters and many abused drugs (Matthes *et al.*, 1996). After activation, MOR is localized to CCPs via its interaction with the adapter protein β -arrestin, after which it undergoes internalization (Moore *et al.*, 2007). This has significant effects on opioid signaling, as cellular sensitivity is directly proportional to the number of receptors available on the cell surface (Martini and Whistler, 2007; Sorkin and von Zastrow, 2009). Further, recent data suggest a definite but complex relationship between the development of opioid addiction and MOR endocytosis, under-

lining its physiological significance (Kim *et al.*, 2008; Koch and Höllt, 2008). Despite this, the mechanisms that regulate MOR endocytosis, especially in the context of the novel cargo-mediated facet of endocytic control, are largely unknown.

Here we use multicolor total internal reflection fluorescence microscopy (TIRFM) to visualize individual events that mediate the endocytosis of MOR in living cells. Using time-resolved imaging and quantitative analysis of these events, we show that MOR localizes to a subset of CCPs and specifically delays their dynamics. Analysis of key components of the four main modules in CME reveals that, unlike PDZ-dependent mechanisms, MOR delays CCPs by controlling the time taken by dynamin to induce scission but not its recruitment. These results reveal a novel facet of how the internalization and desensitization of a key physiologically relevant signaling receptor is regulated and suggest divergent modes for direct control of clathrin-mediated endocytosis by signaling receptor cargo.

RESULTS

MORs localize to a subset of clathrin-coated pits

To analyze the internalization of the MOR at high spatial and temporal resolution, we first optimized an assay to visualize the endocytosis of MOR at the level of individual endocytic events. We tagged MOR with either a FLAG epitope or a pH-sensitive green fluorescent protein (GFP; SpH) at the extracellular N-terminus. SpH ($pK_a \sim 7.1$) is fluorescent at the neutral/alkaline pH of the cell surface but gets rapidly protonated and quenched in acidic environments (Miesenbock *et al.*, 1998; Yudowski *et al.*, 2009). FLAG-tagged MOR was detected using anti-FLAG antibodies tagged to the pH-

insensitive dye Alexa 647. The activation and endocytic trafficking of both of these tagged receptors appeared grossly unchanged compared with untagged receptors, consistent with published reports (Yu *et al.*, 2010). Both SpH-MOR and FLAG-MOR were predominantly distributed on the plasma membrane in HEK293 cells stably expressing the receptors. When observed by live-cell TIRFM, the receptor was relatively diffuse on the plasma membrane before activation and clustered in small, diffraction-limited spots and a few larger structures within 10 s after addition of the MOR-specific agonist [D-Ala², NMe-Phe⁴, Gly-oI⁵]-enkephalin (DAMGO; SpH-MOR shown in Figure 1A; similar results obtained with FLAG-MOR). The diffraction-limited clusters rapidly disappeared with time, consistent with their endocytosis (Supplemental Movie S1). Quantitation of total surface receptor fluorescence over time from multiple cells using wide-field microscopy showed an exponential decrease ($t_{1/2} = 3$ min, $R^2 = 0.9966$) after DAMGO (Figure 1B and solid curve in Supplemental Figure S1B). These rates were consistent with previously reported rates for MOR endocytosis and confirmed by flow cytometry and TIRFM to detect agonist-induced loss of SpH-MOR from

the surface (Supplemental Figure S1, A and C). As expected, SpH and FLAG-MOR showed comparable kinetics of DAMGO-induced endocytosis (Supplemental Figure S1, C and D).

The majority of MOR was endocytosed via the clathrin-mediated pathway. Inhibition of clathrin-mediated endocytosis by Pitstop2 (von Kleist *et al.*, 2011), a selective clathrin inhibitor, effectively inhibited MOR internalization (Supplemental Figure S2, A and C). Similarly, expression of a version of arrestin lacking its clathrin-binding domain (Kang *et al.*, 2009), which still binds the receptor and acts as a dominant negative, also inhibited MOR internalization (Supplemental Figure S2, B and D). To test whether MOR clusters localized to all CCPs, we used dual-color TIRFM to visualize clathrin along with MOR. In cells coexpressing SpH-MOR and dsRed-clathrin, or FLAG-MOR and GFP-clathrin, clathrin fluorescence was seen as distinct puncta on the cell surface before addition of DAMGO, whereas MOR fluorescence was diffuse, similar to Figure 1A (Supplemental Movie S1) without obvious concentration in these puncta. On DAMGO addition, MOR puncta colocalized with CCPs, but only a subset of them, as indicated by CCPs that did not contain a detectable MOR cluster (Supplemental Movie S2 and Figure 1C). Quantitative analysis across multiple cells revealed that 46.5% of the CCPs showed detectable MOR concentration ($n = 290$), defined as a 25% increase in fluorescence over the surrounding membrane (see Supplemental Figure S3). By time-lapse imaging, we followed individual CCPs from their formation to their endocytosis, denoted by abrupt disappearance in the large majority of cases (Supplemental Figure S4), as described previously (Ehrlich *et al.*, 2004; Loerke *et al.*, 2009; Taylor *et al.*, 2011). Strikingly, ~50% of the CCPs never acquired detectable MOR clusters in their entire lifetime (example in Figure 1D and Supplemental Movie S2). This suggests that MOR endocytosis is mediated by a distinct set of CCPs.

MOR extends the lifetime of CCPs in which it clusters

To determine whether MOR exerts cargo-mediated control over CCPs, we compared the dynamics of individual CCPs with MOR and CCPs without detectable MOR. Individual CCPs without detectable MOR were internalized relatively rapidly after their appearance (example in Figure 2A). In contrast, CCPs with MOR stayed noticeably longer on the surface before they disappeared (Figure 2A and Supplemental Movie S2). To quantify this delay, we manually tracked CCPs and calculated their lifetimes. The lifetimes of CCPs were calculated from their initial appearance to the detection of an endocytic event, as evidenced by disappearance, a positional shift, and/or splitting off of clathrin spots (Supplemental Figure S4A). These criteria have been used by our lab and others to detect CCP endocytosis (e.g., Merrifield *et al.*, 2002; Ehrlich *et al.*, 2004; Puthenveedu and von Zastrow, 2006; Loerke *et al.*, 2009; Doyon *et al.*, 2011). Quantitation of >500 CCPs indicated that the distribution of CCP lifetimes before MOR activation was between 20 and 60 s, with the median value being ~35 s. As further verification of this lifetime distribution, we imaged the recruitment of dynamin-GFP into CCPs and its disappearance as an independent index of vesicle scission and endocytosis. Consistent with previous studies (e.g., Merrifield *et al.*, 2002; Puthenveedu and von Zastrow, 2006; Doyon *et al.*, 2011), dynamin fluorescence showed a transient spike just before an endocytic event (Supplemental Figure S4B). Of importance, the lifetime distribution we observed using dynamin fluorescence matched the lifetimes we observed using our criteria for defining endocytosis (Supplemental Figure S4C). Consistent with this, in our experimental system, the majority of CCPs identified showed dynamin recruitment and scission, suggesting that most CCPs were productive. This is consistent with our population distribution centered around the

mean lifetime of ~35 s (Supplemental Figure S4D) and with observations that the absolute CCP lifetimes vary extensively depending on experimental conditions (e.g., Loerke *et al.*, 2009; Saffarian and Kirchhausen, 2009; Batchelder and Yazar, 2010; Nakatsu *et al.*, 2010; Doyon *et al.*, 2011; Mattheyses *et al.*, 2011; Taylor *et al.*, 2011).

To test the effect of MOR clustering without the cell-to-cell variability of absolute lifetime distributions, we quantitated MOR clustering in the same cells before versus after DAMGO. After DAMGO, whereas there were still short-lasting coated pits, many CCPs with lifetimes >90 s were observed, with the median lifetime across the whole population increasing to ~70 s (example cell in Supplemental Figure S5, multiple cells in Figure 2B). A similar increase in the lifetimes of the CCP population was observed also when Imaris was used to detect and track clathrin spots, although the absolute lifetimes differed from those for our manually verified population (Figure 2C). Cumulative distribution graphs of the manually verified lifetimes showed a distinct shift to the right ($k = 37$ s, $R^2 = 0.9932$ before DAMGO vs. $k = 64$ s, $R^2 = 0.9894$ after DAMGO; Figure 2D). To better analyze this at the level of CCP populations, we binned the clathrin lifetimes per cell into 20-s bins. Before MOR clustering, the lifetimes of the majority of CCPs (~50%) fell between 20 and 40 s. In contrast, in the same cells after MOR clustering, a much more diffuse distribution of lifetimes was observed, with each of the bins of longer lifetimes (>60 s) containing 10–20% of CCPs (Figure 2E). As controls, cells imaged for the same period without DAMGO did not show any difference in lifetimes, and DAMGO did not have any effect in cells not expressing MOR (data not shown). This suggests that the delay was not an intrinsic property of CCPs but was induced by MOR clustering.

We next compared the lifetimes of CCPs that showed a detectable MOR cluster, defined as a local increase in fluorescence at least 25% above the surrounding membrane (Supplemental Figure S3), to those that did not. The mean lifetimes of CCPs with MOR clusters (82.2 ± 5.3 s) were noticeably longer than those without clusters (45.3 ± 2.6 s; Figure 2F). To further confirm this objectively, without classifying whether a CCP had a detectable cluster or not, we correlated the raw fluorescence of MOR in CCPs to the corresponding CCP lifetimes. Correlation analysis showed a positive correlation (Spearman $R = 0.35$) between the two parameters, indicating that CCPs with a higher MOR fluorescence showed longer lifetimes (Figure 2G). Taken together, these results indicate that MOR actively delays the surface residence times of the CCPs in which it clusters.

CCP delay by MOR requires two specific leucines on its cytoplasmic tail

To identify the signal on MOR that mediates CCP delay, we first focused on a “bileucine” sequence (LENLEAE) on the C-terminal cytoplasmic tail of MOR that was implicated in its trafficking (Tanowitz and von Zastrow, 2003). To disrupt this sequence, we generated a version of MOR, termed MOR-LLAA, in which the two leucines were mutagenized to alanines. When cells expressing wild-type MOR, MOR-LLAA, or the δ -opioid receptor (DOR, as a negative control for CCP delay; Puthenveedu and von Zastrow, 2006) were activated by the agonist DAMGO (for MOR) or [D-Ala², D-Leu⁵]-enkephalin (DADLE; for DOR), robust receptor clustering was seen in all cases. When the lifetimes of individual receptor clusters were quantitated and compiled, MOR clusters were found to reside approximately twice as long on the surface as DOR clusters (Figure 2H), comparable to B2AR, which was shown to delay CCPs (Puthenveedu and von Zastrow, 2006). Strikingly, the lifetimes of MOR-LLAA clusters were comparable to those of DOR clusters and a version of B2AR in which the PDZ ligand domain was mutated (B2HA [one-way analysis of

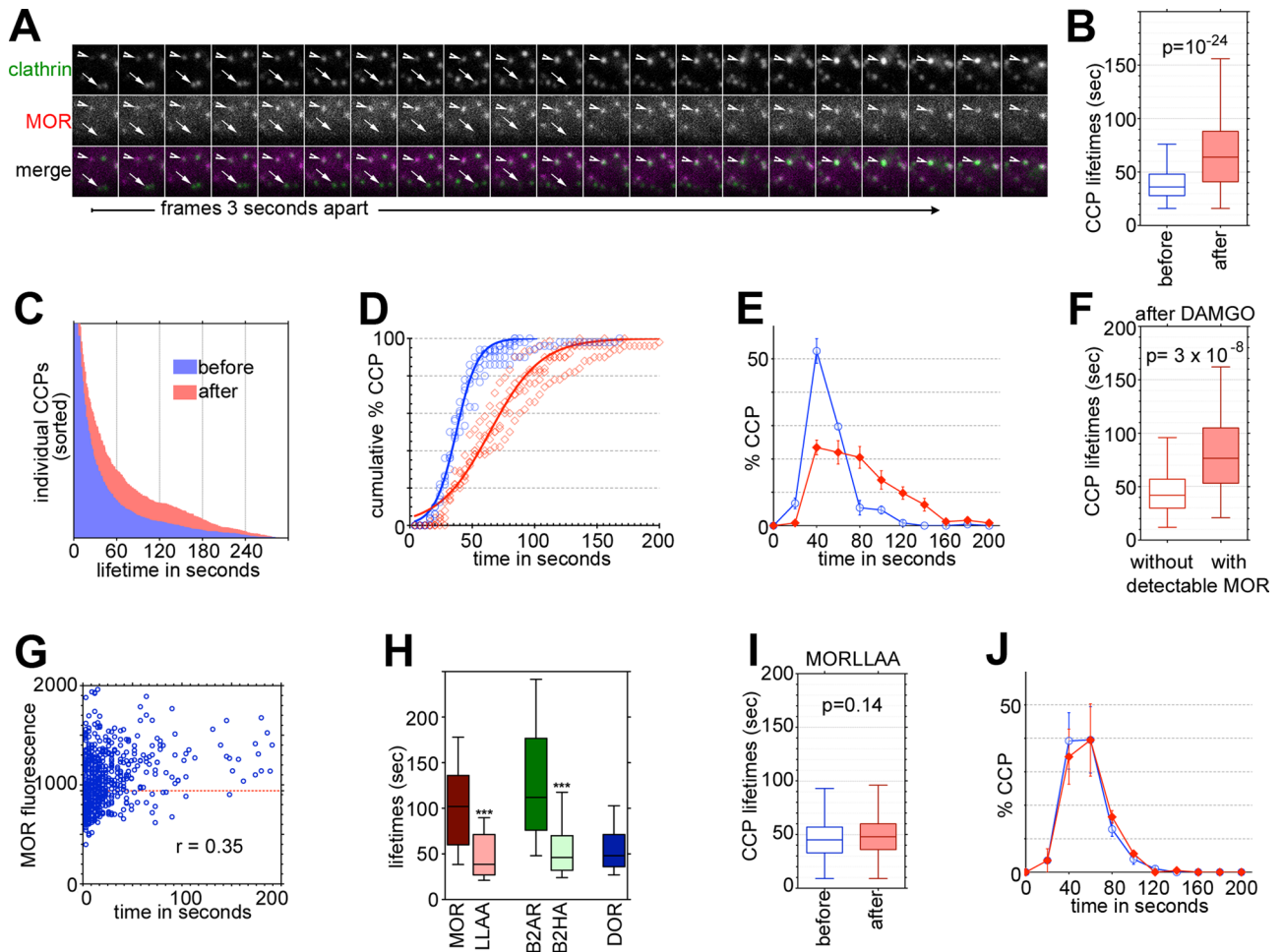


FIGURE 2: MOR extends the lifetime of a subset of CCPs, using a C-terminal “bileucine” sequence. (A) Frames from dual-color TIRFM time series of CCPs, 3 s apart. CCPs containing a detectable MOR cluster (one example shown by arrowhead) lasts a noticeably longer time than a CCP without any (arrows). (B) Box plots showing the range and median of CCP lifetimes in the same cells before vs. after MOR clustering. (C) Sorted lifetimes from >2500 CCPs detected using automated spot detection and tracking before vs. after MOR clustering by DAMGO. Consistent with our conclusions, CCP lifetimes are increased after DAMGO-induced MOR clustering. (D) Example cumulative distribution graphs of CCP lifetimes from five cells before (blue) vs. after (red) MOR clustering. Lines show curve fits across all cells. (E) Lifetimes of clathrin spots on the cell surface, obtained from the same cells before (open blue circles) vs. after (closed red diamonds) MOR clustering, and separated into 20-s bins. (F) Box plots of lifetime of CCPs with detectable MOR clustering vs. those that do not, defined as in Supplemental Figure S3. CCPs with MOR show significantly longer lifetime. (G) Plot of raw MOR fluorescence vs. CCP lifetime, showing positive correlation. The red line shows the estimated cutoff as per Supplemental Figure S3. (H) Surface residence times of individual clusters of MOR, MOR-LLAA, B2AR, B2AR-HA, and DOR after agonist exposure quantitated from multiple cells. Box plots show the median and range. *** $p < 0.0001$ for the mutants compared with wild type. (I) Box plots showing the range and median of CCP lifetime in the same cells before vs. after MOR-LLAA clustering. (J) Clathrin spot lifetime obtained from the same cells before (open blue circles) vs. after (closed red diamonds) MOR-LLAA clustering, fit as in D. There was no observable difference in the CCP lifetime distribution after MOR-LLAA clustering. Box plots are Tukey, and error bars on column graphs are SEM.

variance [ANOVA] not significantly different), indicating that the prolonged surface residence of receptor clusters required the MOR bileucine sequence (Figure 2H). Further, the increased lifetime of CCPs induced by MOR after DAMGO addition was completely abolished in the MOR-LLAA mutant, as seen by quantitating average lifetimes (Figure 2I) and binning the lifetimes of CCP populations to 20-s bins (Figure 2J) as before. Consistent with the change observed in CCP lifetimes, when loss of surface receptor fluorescence was measured over the whole cell, MOR showed both a delay in the initiation of fluorescence loss after DAMGO addition and a slower rate of internalization compared to MOR-LLAA (Supplemental

Figure S6). Taken together, these results indicate that MOR, upon activation with DAMGO, selectively delays the CCPs in which it localizes using a specific bileucine sequence on its C-terminal tail.

MOR delays the vesicle scission phase of CCP endocytosis

We considered four modes by which the bileucine sequence on MOR could delay CCPs: 1) by slowing clathrin assembly; 2) by making larger CCPs, which require more time to assemble; 3) by delaying the recruitment of the scission machinery; or 4) by regulating the activity of the scission machinery. To test the first possibility, we first measured the fluorescence traces of clathrin over time in CCPs

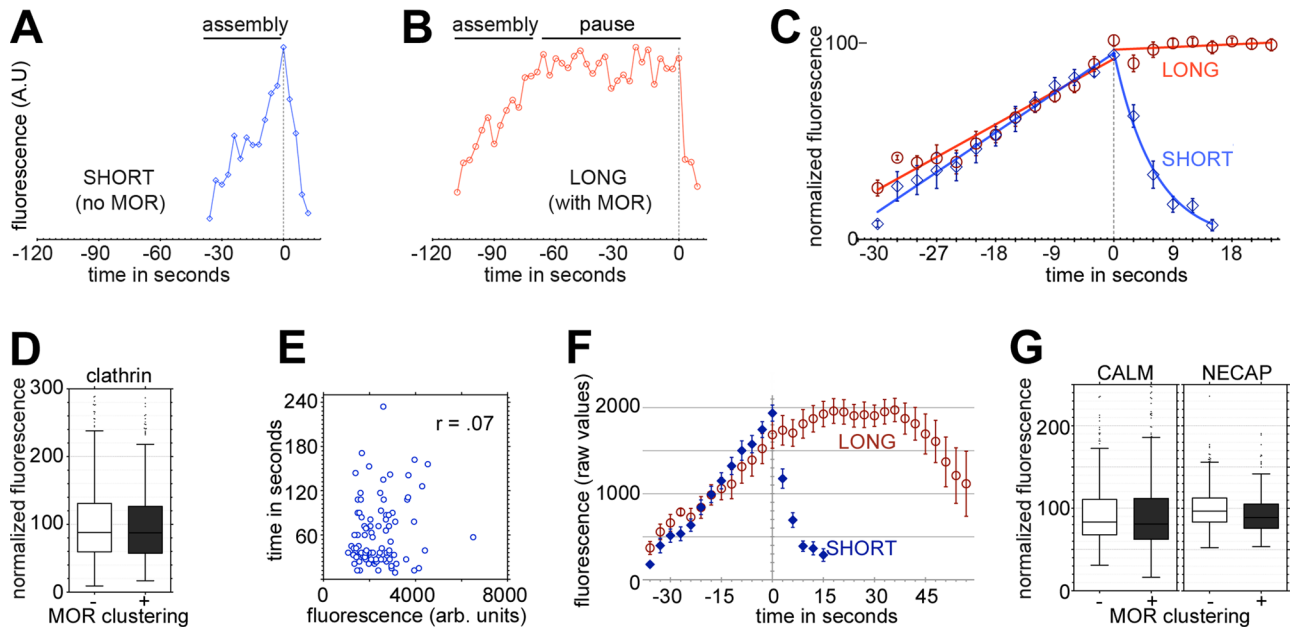


FIGURE 3: MOR pauses CCP progression after clathrin assembly. (A) Example traces of clathrin fluorescence over time from short CCPs (lifetime, 30–40 s) without MOR and long CCPs (>75 s, see text) with MOR clusters. The short CCPs showed a linear increase in fluorescence, followed by a rapid decrease characteristic of scission and endocytosis. The long CCPs showed a distinct “pause” after near-maximum clathrin fluorescence, before endocytosis. (C) Averaged normalized fluorescence from 20 short and long CCPs aligned to their initial appearance. The slopes of assembly are not significantly different. (D) Tukey box plots of maximum clathrin fluorescence calculated from CCPs without MOR vs. CCPs with MOR across the same set of cells after DAMGO-induced MOR clustering. Values normalized to the average value without MOR show no significant difference between the two populations ($n > 350$ in each case). (E) Correlation between peak clathrin fluorescence and lifetime ($n = 100$), showing no correlation between these criteria. (F) Average fluorescence values from traces across 20 short and long CCPs show roughly the same peak fluorescence before endocytosis across both populations. (G) Tukey box plots of maximum fluorescence values of CALM and NECAP before vs. after DAMGO-induced MOR clustering, showing no difference.

containing MOR clusters and compared them to CCPs devoid of MOR. Before MOR clustering, and in CCPs devoid of MOR, clathrin fluorescence in most CCPs showed a linear increase, denoting clathrin coat assembly, followed by a sharp decrease corresponding to scission and movement of vesicles away from the cell surface (example in Figure 3A). This fluorescence signature was largely consistent with previous observations (Merrifield *et al.*, 2002; Ehrlich *et al.*, 2004; Mettlen *et al.*, 2010; Henry *et al.*, 2012). In contrast, in the longer-lasting CCPs containing detectable MOR clusters that were observed after exposure to agonist in the same cells, clathrin showed a similar linear increase, followed by a plateau phase in which there was no further increase, before the rapid loss of fluorescence (example in Figure 3B). This suggested that the assembly of the clathrin cage was not affected, and MOR “paused” further progression of CCP endocytosis after clathrin assembly was complete. Further, to quantitatively estimate the rate assembly of clathrin, we classified CCPs into short (no detectable MOR cluster) and long (with MOR clusters) CCPs. We defined a short CCP as having a lifetime of between 30 and 40 s, which approximated the median lifetime of CCPs before MOR activation (Figure 2 and Supplemental Figure S5). We defined a long CCP as having a lifetime of >75 s. By manual verification of CCP lifetimes, this was over the 90th percentile of CCP lifetimes observed before MOR clustering (e.g., Figure 2D). When aligned to the time frame in which we first detected clathrin, taken as the initiation of clathrin assembly, the fluorescence traces roughly fit to a linear regression ($R^2 = 0.73$ and 0.68 , respectively, for short and long CCPs). Of importance, the slopes in the

assembly phase showed no significant difference ($p = 0.12$; pooled slope, 2.2; pooled $y_{\text{int}} = 98$; Figure 3C), indicating that the assembly of clathrin was not changed.

To test the second possibility, we compared the peak clathrin fluorescence values in CCPs containing MOR with CCPs without detectable MOR, as an index of the total clathrin present and therefore the size of vesicles formed. We first measured the clathrin fluorescence in CCPs of maximum-intensity projections of time series. As shown in Figure 3D, there was no statistically significant difference ($p = 0.55$) in the clathrin fluorescence between these CCPs with and without detectable MOR. Consistent with this, we observed no correlation between peak clathrin fluorescence and CCP lifetimes (Figure 3E; Spearman $R = 0.07$, $p = 0.45$). In addition, we monitored the clathrin fluorescence over time from multiple example CCPs with and without MOR clusters (defined as in Supplemental Figure S3) and examined the peak values of fluorescence of clathrin in these traces. The average fluorescence traces showed no significant difference in the maximum clathrin fluorescence before endocytosis (Figure 3F), indicating that MOR-containing CCPs are not larger. We also observed no difference in the peak fluorescence of adaptin ear-binding clathrin-associated protein (NECAP) and clathrin assembly lymphoid myeloid leukemia protein (CALM; Figure 3G, $p = 0.25$ for NECAP and 0.31 for CALM), the two main proteins shown to affect the size of clathrin-coated vesicles (Zhang *et al.*, 1998; Meyerholz *et al.*, 2005; Ritter *et al.*, 2007; Maritzen *et al.*, 2012). Further, the lifetimes of NECAP and CALM were not changed by MOR clustering (Supplemental Figure S7, A and C). Of interest, the absolute

lifetime of CALM was increased upon coexpression of clathrin, and, although there was a slight increase in the lifetime after DAMGO, this did not match the increase in clathrin lifetime (Supplemental Figure S7B). Of interest, although CALM has been reported to follow clathrin dynamics, we observed that, in longer-lasting CCPs, CALM fluorescence was dissociated from clathrin fluorescence before endocytosis (Supplemental Figure S7D). Taken together, however, our results suggest that the clathrin assembly and vesicle size were not affected by MOR clustering.

To test the third and fourth possibilities, we directly imaged the behavior of dynamin, a key protein in scission. Cells expressing FLAG-MOR, dynamin-GFP, and clathrin-dsRed were imaged for 5 min before and 5 min after addition of DAMGO to detect whether DAMGO-induced MOR clustering altered the behavior of dynamin. Before DAMGO addition, dynamin was recruited just before scission in CCPs, as previously observed. After DAMGO addition, consistent with MOR clustering in a subset of CCPs, we observed that ~30% of dynamin puncta did not colocalize with MOR (e.g., arrows in Figure 4A). Strikingly, in CCPs paused by MOR, dynamin was observed for a significantly longer time than in CCPs devoid of MOR (example in Figure 4B). This was apparent when the behavior of dynamin puncta was compared in the same cells before versus after MOR clustering by DAMGO. As shown in the example kymograph for the same cells before versus after DAMGO-induced MOR clustering (Figure 4C), dynamin stays in CCPs much longer after DAMGO. Quantitation of multiple CCPs indicated that the average dynamin lifetime doubled, from 7 to 14 s, after DAMGO-induced MOR clustering (Figure 4D). This increase required the interactions of the C-terminal leucines on MOR, as clustering of MOR-LLAA did not change dynamin lifetimes (Figure 4D). This increase in dynamin lifetime was further confirmed by triple-color live-cell TIRFM of clathrin, dynamin, and MOR (Supplemental Movie S3). Fluorescence traces from individual CCPs showed that in CCPs showing a detectable increase in MOR fluorescence over background, dynamin was recruited and persisted for a longer period before scission (example trace in Figure 4E, left). In contrast, in CCPs without MOR clusters (where MOR fluorescence stayed at the baseline), dynamin showed the characteristic spike just before scission (Figure 4E, right). When dynamin lifetimes from MOR-expressing cells before versus after DAMGO were binned into 9 s bins, the frequency histogram showed a noticeable shift to longer lifetimes after DAMGO exposure (Figure 4F, left). This shift was absent in MOR-LLAA-expressing cells. Consistent with this, dynamin was typically recruited at or after the end of the assembly phase of clathrin in CCPs with MOR and persisted through the “pause” phase until scission (example in Figure 4G).

To test whether the delay correlated with an increased amount of dynamin required to cause CCP scission, we quantified by maximum-intensity projections of time series the peak fluorescence of dynamin in each CCP as an index of the amount of dynamin. When compared with CCPs before DAMGO-mediated MOR clustering, CCPs after MOR clustering showed no significant change ($4 \pm 4.2\%$, $p = 0.36$) in dynamin fluorescence (Figure 4H). Taken together with the normal recruitment and increased lifetime of dynamin, these results suggest that MOR delays CCPs lifetime by acting primarily on the vesicle scission module of clathrin-mediated endocytosis (Figure 4I).

DISCUSSION

Cargo-mediated control of individual CCPs is an emerging concept that can potentially explain how cells can selectively control the endocytosis of multiple cargo proteins using shared core trafficking proteins (Puthenveedu and von Zastrow, 2006). In this study, we identify MOR, the main target of opioid neurotransmitters and many

clinically abused drugs, as a physiologically relevant signaling cargo that can control dynamics of individual CCPs through interactions of its C-terminal tail.

The dynamical behavior of CCPs has been recorded extensively using live-cell TIRFM (e.g., Loerke *et al.*, 2009; Doyon *et al.*, 2011; Taylor *et al.*, 2011). The range of CCP lifetimes we observe in HEK293 cells broadly match these careful and exhaustive studies. One notable difference is that, in contrast to recent published data using automated detection of CCPs, we do not see a significant fraction of short-lasting “abortive” CCPs (Figure 2E). Consistent with this, most of the CCPs we observe recruit dynamin and undergo scission (Supplemental Figure S4). It is possible that this reflects differences in detection methods, cell types, or experimental conditions. It has become increasingly clear that the dynamics of individual components and CCP modules in mammalian cells vary highly based on their expression levels, the cell types used, temperature, and imaging conditions (Merrifield *et al.*, 2002; Ehrlich *et al.*, 2004; Puthenveedu and von Zastrow, 2006; Loerke *et al.*, 2009; Saffarian and Kirchhausen, 2009; Batchelder and Yarar, 2010; Nakatsu *et al.*, 2010; Doyon *et al.*, 2011; Mattheyses *et al.*, 2011; Taylor *et al.*, 2011; Henry *et al.*, 2012). Variations in culture conditions, such as membrane tension, might also alter the biochemical requirements for endocytosis (Boulant *et al.*, 2011). An additional consideration is that TIRFM visualizes primarily the bottom surface of the cell, which is attached to a secreted extracellular matrix (ECM) on the coverslip. Clathrin generates defined CCPs, as well as larger and pleiomorphic “plaques” on this surface, and the morphology and dynamics of these plaques are distinct from those of CCPs (Saffarian and Kirchhausen, 2009). However, the dynamics of CCPs on the bottom and the top surfaces seem broadly similar (Saffarian and Kirchhausen, 2009). Although it is arguable as to which surface best represents the membranes of cells in a three-dimensional ECM, such as neurons in the brain, extensive data suggest that GPCRs robustly cluster in response to agonists on both the attached and the free surface (Goodman *et al.*, 1996; Santini *et al.*, 1998; Shenoy *et al.*, 2007; N’Diaye *et al.*, 2008).

Although these methodological constraints are certainly to be noted, we believe that the differences in CCP lifetimes we observe after MOR activation are unlikely to be a result of such changes. First, the changes we see are acute and are observed seconds after agonist addition (Figure 2, B–E). Second, the changes are largely restricted to CCPs that show detectable MOR concentration over background (Figure 2, F and G). Third, these changes are not seen with related GPCRs such as DOR and are abolished by mutating two residues on MOR (MOR-LLAA, Figure 2, H–J). Fourth, there is a detectable difference in endocytic kinetics between MOR and MOR-LLAA, even in assays not restricted to the bottom surface of the cell (Supplemental Figure S6). Fifth, we restricted our analyses to diffraction-limited spots that we can resolve as appearing and disappearing within the time frame of the movie, thereby excluding the majority of plaques. Taken together, therefore, although the absolute lifetimes that we propose might vary depending on experimental conditions, our results support the conclusion that clustering of MOR in CCPs acutely pauses CCPs, indicating cargo-mediated regulation of CCP behavior by MOR.

How does MOR pause CCPs? Our results suggest that this requires clustering of MOR into CCPs and that this is not a general downstream effect of MOR signaling. First, the increase in lifetime was restricted to a subset of CCPs (Figure 2, B and E). Second, only the subset of CCPs containing detectable MOR clusters showed a noticeable increase in lifetime (Figure 2F). Third, the increase in CCP lifetime correlated with the intensity of MOR clusters (Figure 2G).

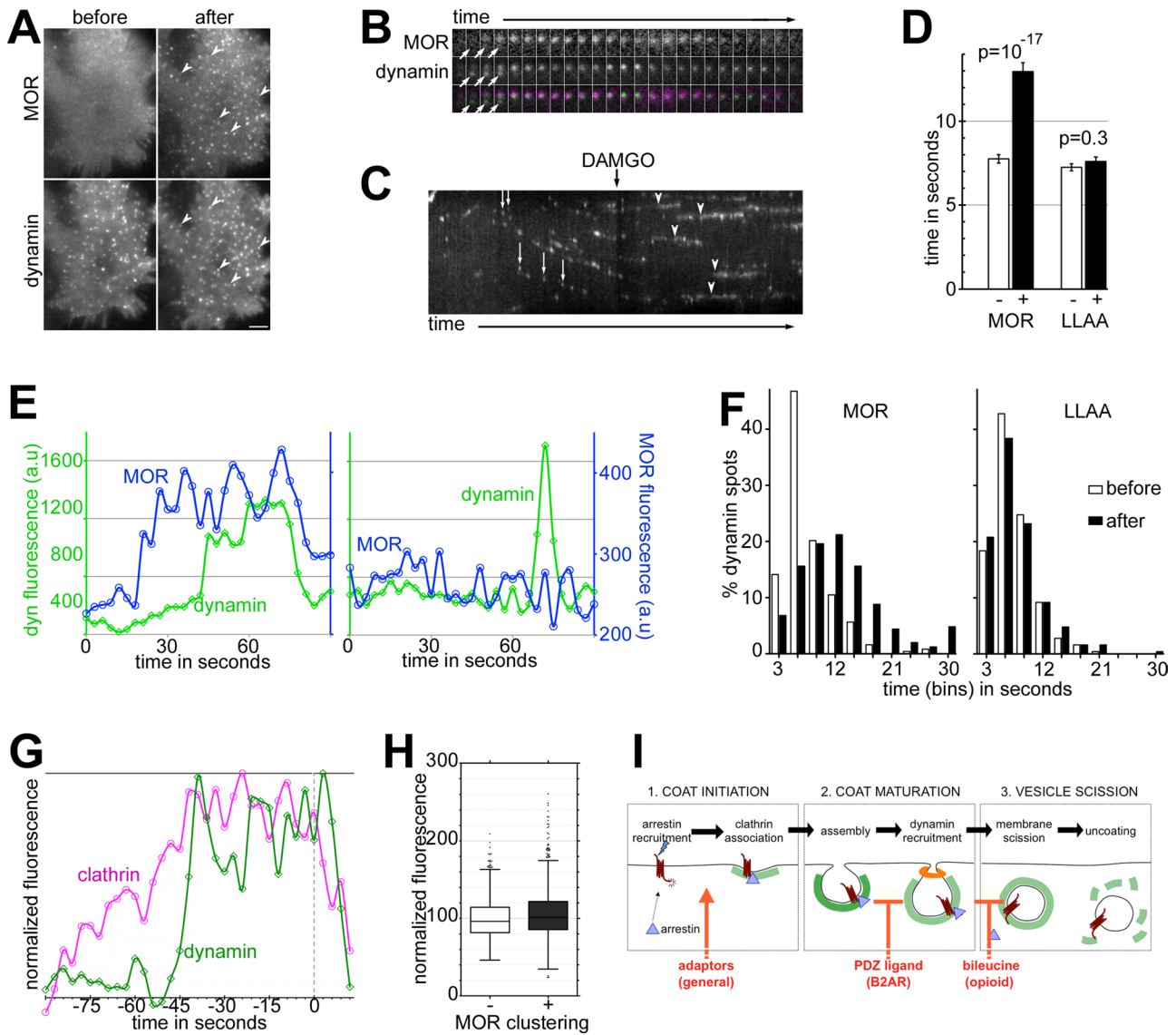


FIGURE 4: MOR pauses CCPs by delaying the endocytic scission module. (A) Maximum-intensity projection of 30 s of a time-lapse movie from an example cell expressing MOR and dynamin-GFP before and after DAMGO. Arrowheads show example dynamin spots without MOR. Scale bar, 5 μ m. (B) Example frames from a time series 3 s apart, showing two CCPs with dynamin, one with MOR, and one without (arrows). The dynamin in the CCP with MOR lasts significantly longer than in the CCP without MOR. (C) Kymograph from a region of a cell imaged 5 min before and 5 min after DAMGO. Dynamin lasts just one or two frames before DAMGO (“spots” denoted by arrows) and much longer (“lines” denoted by arrowheads) after DAMGO. The region of the cell from which the kymograph is shown is noted in Supplemental Figure S8. (D) Average dynamin lifetime in cells expressing MOR or MOR-LLAA before vs. after DAMGO ($n > 250$ in each case). The increase in dynamin lifetime seen after DAMGO with MOR is lost with MOR-LLAA. Error bars are SEM. (E) Traces of raw fluorescence of FLAG-MOR and dynamin from example CCPs. Dynamin fluorescence stays noticeably longer in the cell showing a MOR cluster. (F) Lifetimes of dynamin spots obtained from the cells expressing MOR (left) or MOR-LLAA (right) before (open bars) and after (solid bars) MOR clustering, were separated into 9 s bins. In MOR-expressing cells, but not MOR-LLAA cells, dynamin distributions shifted to longer lifetimes after DAMGO. (G) Fluorescence trace of clathrin and dynamin, normalized to the maximum, from an example CCP containing MOR. Dynamin localizes near the end of the assembly phase and lasts through the pause phase. (H) Tukey box plots of dynamin fluorescence in CCPs with vs. without MOR, normalized to CCPs without MOR ($n > 1100$ in each case). (I) Model for divergent modes of cargo-mediated control of endocytosis by signaling receptors.

Fourth, the delay was dependent on a specific sequence motif on the C-terminal tail of MOR (Figure 2, H–J). The last two observations suggest a stoichiometric effect of interactions of the MOR tail in pausing CCPs. Locally clustered MOR possibly regulates the activity of the scission module of endocytosis (Figure 4) without affecting the clathrin assembly rate, the total amount of clathrin, or the re-

ruitment of dynamin (Figure 3). In MOR-containing CCPs, we observed dynamin recruitment after the end of the clathrin assembly phase at various points in the pause phase (examples in Figure 4, E and G). However, once dynamin was recruited, its lifetime was significantly increased in MOR-containing CCPs (Figure 4, D and F). We cannot rule out an additional effect of MOR on the recruitment of

the dynamin scission machinery, as the delay in dynamin lifetimes does not precisely match the increased CCP lifetimes. However, our results suggest an active role for interactions of the C-terminal “bileucine” domain of MOR in pausing the progress of CCPs to vesicle scission even after recruitment of the scission machinery.

This provides a novel example for regulation of CCP lifetimes by a GPCR and suggests that cargo-mediated regulation is a general mode of endocytic control by signaling receptors. GPCRs likely work in both initiating CCPs via clustering of the cargo adapters arrestin and AP2 (Santini *et al.*, 1998) and in controlling the dynamics of later steps in CCP assembly and scission. The only other known example of cargo-mediated control by a signaling receptor, B2AR, delayed CCPs using local interactions of its C-terminal PDZ-interacting domain to the cytoskeleton (Puthenveedu and von Zastrow, 2006). Several observations suggest that MOR uses a mechanism distinct from that of B2AR for pausing CCPs. B2AR significantly delayed the recruitment of dynamin, whereas MOR did not. Once dynamin was recruited, B2AR did not affect the time it took to cause vesicle scission, whereas MOR significantly delayed its lifetime (Figure 4, D–G). Further, MOR does not have an identified PDZ ligand, nor is there any evidence that the cytoplasmic tail of MOR can interact with actin. Taken together, these results suggest that GPCRs can control endocytosis at least at two separate points, with B2AR delaying recruitment of dynamin and MOR pausing CCPs after dynamin recruitment (Figure 4I).

Recent evidence also suggests that different modules in the CCP cycle are cooperative and that there is complex feedback between dynamin, actin, and other CCP components that act during fission (Shin *et al.*, 2008; Ferguson *et al.*, 2009; Taylor *et al.*, 2012; Meinecke *et al.*, 2013). It is not clear how any of these observed mechanisms modify dynamin lifetimes. One possibility is that MOR modifies dynamin’s GTPase activity, as proposed for the adapter protein TTP (Tosoni *et al.*, 2005). However, because dynamin is an assembly-regulated GTPase, its regulation is likely to involve multiple input mechanisms (Schmid and Frolov, 2011; Ferguson and De Camilli, 2012). This leads to the alternate possibility that MOR coordinates the cooperative feedback between different CCP modules as opposed to the activity of a single component. This might include the scission, uncoating, and actin machineries. In any case, along with PDZ ligands, this suggests multiple divergent cargo-mediated checkpoints in the CCP cycle that control vesicle scission. In combination with the segregation of receptor cargo into distinct CCPs and ubiquitin-based biochemical checkpoints that ensure sufficient cargo concentration before scission (Henry *et al.*, 2012), cargo-mediated tuning of CCP dynamics may provide a method for obtaining virtually unlimited selective control over the internalization of different GPCR cargo.

Such cargo-mediated regulation likely has significant physiological consequences on cellular signaling by GPCRs. The outcomes of receptor endocytosis on cellular sensitization to signals are well established (e.g., reviewed in Martini and Whistler, 2007; Sorkin and von Zastrow, 2009). In addition to the initial G-protein-mediated signaling, many GPCRs can induce a distinct signaling pathway after they bind arrestin (Lefkowitz and Shenoy, 2005; Calebiro *et al.*, 2009). Arrestin association with the plasma membrane is sufficient to induce this mode of signaling, and, in the case of GPCR-mediated recruitment of arrestin, the relative strengths of these different phases of signaling often depend on the activating ligand (Terrillon *et al.*, 2004; Reiter *et al.*, 2012). In the case of MOR, arrestin is released immediately upon vesicle scission, suggesting that cargo-mediated signaling might control the second phase of GPCR signaling. Considering that practically all known GPCRs share common

trafficking components, including arrestin (Pierce *et al.*, 2002; Hanyaloglu and von Zastrow, 2008), and that multiple receptors are activated concomitantly in many cells, the dynamics of individual CCPs may therefore determine the extent of each phase of signaling by controlling the time that each receptor spends bound to each signaling complex (e.g., arrestin). The divergent modes of CCP regulation identified here therefore likely are a critical aspect of normal signal integration, as they can maintain selective control over different phases of signaling pathways evoked by GPCRs.

Although our studies were performed in heterologous systems expressing exogenous receptors, such systems have been established as excellent models to study the molecular mechanisms underlying GPCR behavior, and the principles identified have largely been validated in more complex systems (Pierce *et al.*, 2002; Hanyaloglu and von Zastrow, 2008; Marchese *et al.*, 2008; Magalhaes *et al.*, 2012). The fact that we observe CCP regulation by exogenous GPCRs in HEK293 cells suggests that these cells have the required machinery for cargo-mediated control of CCPs and, of importance, that CCP delay is likely a general mechanism across cell types. However, although it is clear that GPCRs cluster and internalize in the brain *in vivo*, the extent of CCP regulation by MOR and related GPCRs in the brain, especially in the context of endogenous levels of receptors, and whether there are distinct physiological consequences in these cells, remain to be tested.

At the broad cell biological level, our results suggest that cargo molecules in general are far more active players in endocytosis than was previously appreciated. Some cargo can nucleate and stabilize CCPs early (Ehrlich *et al.*, 2004; Loerke *et al.*, 2009), arguably without affecting further dynamics of stabilized CCPs, whereas others can control CCP dynamics by regulating key core components (Tosoni *et al.*, 2005; Puthenveedu and von Zastrow, 2006; Mettlen *et al.*, 2010). Sequestration of cargo in subsets of CCPs, followed by regulation of those CCPs by *cis*-sequence determinants on the cargo molecules themselves, allows for nearly unlimited biochemical and functional specialization of CCPs that otherwise share the same trafficking proteins. Emerging data suggest that, in addition to CCPs, GPCR cargo can also influence trafficking at the endosome by regulating the kinetics of the Rab4-dependent recycling pathway (Yudowski *et al.*, 2009). Such functional specialization of trafficking microdomains, generated on demand and regulated by cargo proteins themselves, might provide a general theme to explain the long-standing question as to how cells can constantly transport hundreds of different cargo using shared trafficking components without significant competition and inhibition among different proteins.

MATERIALS AND METHODS

Constructs, cell, and reagents

Tagged dynamin, clathrin, cortactin, and MOR constructs were described earlier (Puthenveedu and von Zastrow, 2006; Puthenveedu *et al.*, 2010; Yu *et al.*, 2010). CALM- and NECAP-mCherry constructs were purchased from Addgene (Cambridge, MA; Taylor *et al.*, 2011). HEK 293 cells (American Type Culture Collection, Manassas, VA) stably expressing either SSF-MOR or SpH-MOR and mutants were generated by selection using Geneticin or Zeocin (Invitrogen, Carlsbad, CA) as per manufacturer’s instructions. Components of the endocytic machinery were transiently transfected using Effectene (Qiagen, Valencia, CA), and imaged 3–5 d after transfection. Cells were maintained in DMEM with 10% fetal bovine serum (FBS). DAMGO, DADLE, and isoproterenol were purchased from Sigma-Aldrich (St. Louis, MO) and used at 10 μ M from a 10 mM frozen stock. Pitstop 2 was purchased from Abcam (Cambridge, MA).

Microscopy and image analysis

Cells were imaged using a Nikon Eclipse Ti automated inverted microscope (Nikon, Melville, NY) equipped for through-the-objective TIRFM and outfitted with a temperature-, humidity-, and CO₂-controlled chamber. Images were acquired with an iXon+ 897 electron-multiplying charge-coupled device camera with solid-state lasers of 488, 561, and 647 nm as light sources. The cells were imaged live in Opti-MEM (Invitrogen) with 30 mM 4-(2-hydroxyethyl)-1-piperazineethanesulfonic acid and 10% FBS, using a 100× or 60×/1.45 numerical aperture TIRF objective (Nikon). Time-lapse movies were collected as tiff stacks and analyzed in ImageJ (National Institutes of Health, Bethesda, MD). For estimating surface receptor fluorescence, SpH-MOR or labeled SSF-MOR cells were imaged for 5 min before DAMGO and 5 min after DAMGO, capturing every 3 s. A 50 × 50-pixel box in the center of the cell was used to measure fluorescence changes over time to avoid errors due to changes in cell shape. CCP lifetimes were estimated as described (Puthenveedu and von Zastrow, 2006). Peak fluorescence values of clathrin or dynamin were measured by either of two methods. To analyze a larger number of CCPs, maximum-intensity projections of time-lapse movies corresponding to 15 s each taken before versus after exposure to DAMGO from multiple cells were analyzed to detect CCPs containing MOR clusters. The corresponding clathrin or dynamin fluorescence was compared with CCPs in the same cells that did not colocalize with MOR clusters. The box plots shown represent cumulated data from >500 CCPs from multiple cells in each case. For obtaining *p* values, average values were calculated from individual cells, and a *t* test was performed across the averages obtained from multiple cells in the two different conditions. These measurements were further confirmed by tracking the fluorescence values of multiple individual CCPs over time and detecting the peak fluorescence values in these CCPs over their entire lifetimes. Kymographs were obtained by reslicing a region of the cell and maximum-intensity projections. Automated tracking of CCPs was performed on the same data sets using the Spots function in Imaris (Bitplane, Zurich, Switzerland) to detect clathrin fluorescence, and MOR fluorescence was measured on each of these tracks. Raw data sets are shown. These tracks were manually verified in a few cases to explain the difference between the lifetimes observed. All fluorescence quantitations were done on images directly acquired from the camera with no manipulation or adjustments. Simple image math and statistical analyses were done using Excel (Microsoft, Redmond, WA), and curve fits and ANOVA were done using Prism (GraphPad Software, La Jolla, CA).

ACKNOWLEDGMENTS

We thank S. Bowersox and C. Almaguer for technical help and comments on the manuscript and M. von Zastrow for essential advice, help, and reagents; A. D. Linstedt, T. H. Lee, S. Mukhopadhyay, G. Romero, P. Friedman, and P. McPherson for advice and critique; C. Szalinski for help with Imaris; and D. Shiwerski, R. Vistein, B. Kumcuoglu, and A. G. Henry for valuable comments, help, and discussion. This work was supported by National Institutes of Health Grant DA024698 to M.A.P.

REFERENCES

- Batchelder EM, Yarar D (2010). Differential requirements for clathrin-dependent endocytosis at sites of cell-substrate adhesion. *Mol Biol Cell* 21, 3070–3079.
- Boettner DR, Chi RJ, Lemmon SK (2012). Lessons from yeast for clathrin-mediated endocytosis. *Nat Cell Biol* 14, 2–10.
- Boulant S, Kural C, Zehe JC, Ubelmann F, Kirchhausen T (2011). Actin dynamics counteract membrane tension during clathrin-mediated endocytosis. *Nat Cell Biol* 13, 1124–1131.
- Calebiro D, Nikolaev VO, Gagliani MC, de Filippis T, Dees C, Tacchetti C, Persani L, Lohse MJ (2009). Persistent cAMP-signals triggered by internalized G-protein-coupled receptors. *PLoS Biol* 7, e1000172.
- Doyon JB *et al.* (2011). Rapid and efficient clathrin-mediated endocytosis revealed in genome-edited mammalian cells. *Nat Cell Biol* 13, 331–337.
- Ehrlich M, Boll W, Van Oijen A, Hariharan R, Chandran K, Nibret ML, Kirchhausen T (2004). Endocytosis by random initiation and stabilization of clathrin-coated pits. *Cell* 118, 591–605.
- Ferguson SM, De Camilli P (2012). Dynamin, a membrane-remodelling GTPase. *Nat Rev Mol Cell Biol* 13, 75–88.
- Ferguson SM *et al.* (2009). Coordinated actions of actin and BAR proteins upstream of dynamin at endocytic clathrin-coated pits. *Dev Cell* 17, 811–822.
- Goodman OBJ, Krupnick JG, Santini F, Gurevich VV, Penn RB, Gagnon AW, Keen JH, Benovic JL (1996). Beta-arrestin acts as a clathrin adaptor in endocytosis of the beta2-adrenergic receptor. *Nature* 383, 447–450.
- Hanyaloglu AC, von Zastrow M (2008). Regulation of GPCRs by endocytic membrane trafficking and its potential implications. *Annu Rev Pharmacol Toxicol* 48, 537–568.
- Henry AG, Hislop JN, Grove J, Thorn K, Marsh M, von Zastrow M (2012). Regulation of endocytic clathrin dynamics by cargo ubiquitination. *Dev Cell* 23, 519–532.
- Kaksonen M, Peng HB, Rauvala H (2000). Association of cortactin with dynamic actin in lamellipodia and on endosomal vesicles. *J Cell Sci* 113, Pt 244421–4426.
- Kang DS, Kern RC, Puthenveedu MA, von Zastrow M, Williams JC, Benovic JL (2009). Structure of an arrestin2-clathrin complex reveals a novel clathrin binding domain that modulates receptor trafficking. *J Biol Chem* 284, 29860–29872.
- Keith DE, Murray SR, Zaki PA, Chu PC, Lissin DV, Kang L, Evans CJ, von Zastrow M (1996). Morphine activates opioid receptors without causing their rapid internalization. *J Biol Chem* 271, 19021–19024.
- Kelly BT, Owen DJ (2011). Endocytic sorting of transmembrane protein cargo. *Curr Opin Cell Biol* 23, 404–412.
- Kim JA *et al.* (2008). Morphine-induced receptor endocytosis in a novel knockin mouse reduces tolerance and dependence. *Curr Biol* 18, 129–135.
- Koch T, Höllt V (2008). Role of receptor internalization in opioid tolerance and dependence. *Pharmacol Ther* 117, 199–206.
- Lefkowitz RJ, Shenoy SK (2005). Transduction of receptor signals by beta-arrestins. *Science* 308, 512–517.
- Loerke D, Mettlen M, Yarar D, Jaqaman K, Jaqaman H, Danuser G, Schmid SL (2009). Cargo and dynamin regulate clathrin-coated pit maturation. *PLoS Biol* 7, e57.
- Magalhaes AC, Dunn H, Ferguson SS (2012). Regulation of GPCR activity, trafficking and localization by GPCR-interacting proteins. *Br J Pharmacol* 165, 1717–1736.
- Marchese A, Paing MM, Temple BR, Trejo J (2008). G protein-coupled receptor sorting to endosomes and lysosomes. *Annu Rev Pharmacol Toxicol* 48, 601–629.
- Maritzen T, Koo SJ, Haucke V (2012). Turning CALM into excitement: AP180 and CALM in endocytosis and disease. *Biol Cell* 104, 588–602.
- Martini L, Whistler JL (2007). The role of mu opioid receptor desensitization and endocytosis in morphine tolerance and dependence. *Curr Opin Neurobiol* 17, 556–564.
- Matthes HW *et al.* (1996). Loss of morphine-induced analgesia, reward effect and withdrawal symptoms in mice lacking the mu-opioid-receptor gene. *Nature* 383, 819–823.
- Mattheyses AL, Atkinson CE, Simon SM (2011). Imaging single endocytic events reveals diversity in clathrin, dynamin and vesicle dynamics. *Traffic* 12, 1394–1406.
- McMahon HT, Boucrot E (2011). Molecular mechanism and physiological functions of clathrin-mediated endocytosis. *Nat Rev Mol Cell Biol* 12, 517–533.
- Meinecke M, Boucrot E, Camdere G, Hon WC, Mittal R, McMahon HT (2013). Cooperative recruitment of dynamin and BIN/amphiphysin/Rvs (BAR) domain-containing proteins leads to GTP-dependent membrane scission. *J Biol Chem* 288, 6651–6661.
- Merrifield CJ, Feldman ME, Wan L, Almers W (2002). Imaging actin and dynamin recruitment during invagination of single clathrin-coated pits. *Nat Cell Biol* 4, 691–698.
- Mettlen M, Loerke D, Yarar D, Danuser G, Schmid SL (2010). Cargo- and adaptor-specific mechanisms regulate clathrin-mediated endocytosis. *J Cell Biol* 188, 919–933.

- Meyerholz A, Hinrichsen L, Groos S, Esk PC, Brandes G, Ungewickell EJ (2005). Effect of clathrin assembly lymphoid myeloid leukemia protein depletion on clathrin coat formation. *Traffic* 6, 1225–1234.
- Miesenbock G, De Angelis DA, Rothman JE (1998). Visualizing secretion and synaptic transmission with pH-sensitive green fluorescent proteins. *Nature* 394, 192–195.
- Moore CA, Milano SK, Benovic JL (2007). Regulation of receptor trafficking by GRKs and arrestins. *Annu Rev Physiol* 69, 451–482.
- Nakatsu F, Perera RM, Lucast L, Zoncu R, Domin J, Gertler FB, Toomre D, De Camilli P (2010). The inositol 5-phosphatase SHIP2 regulates endocytic clathrin-coated pit dynamics. *J Cell Biol* 190, 307–315.
- N'Diaye EN, Hanyaloglu AC, Kajihara KK, Puthenveedu MA, Wu P, von Zastrow M, Brown EJ (2008). The ubiquitin-like protein PLIC-2 is a negative regulator of G protein-coupled receptor endocytosis. *Mol Biol Cell* 19, 1252–1260.
- Pierce KL, Premont RT, Lefkowitz RJ (2002). Seven-transmembrane receptors. *Nat Rev Mol Cell Biol* 3, 639–650.
- Puthenveedu MA, Lauffer B, Temkin P, Vistein R, Carlton P, Thorn K, Taunton J, Weiner OD, Parton RG, von Zastrow M (2010). Sequence-dependent sorting of recycling proteins by actin-stabilized endosomal microdomains. *Cell* 143, 761–773.
- Puthenveedu MA, von Zastrow M (2006). Cargo regulates clathrin-coated pit dynamics. *Cell* 127, 113–124.
- Rao Y, Rückert C, Saenger W, Haucke V (2012). The early steps of endocytosis: from cargo selection to membrane deformation. *Eur J Cell Biol* 91, 226–233.
- Reiter E, Ahn S, Shukla AK, Lefkowitz RJ (2012). Molecular mechanism of β -arrestin-biased agonism at seven-transmembrane receptors. *Annu Rev Pharmacol Toxicol* 52, 179–197.
- Ritter B, Denisov AY, Philie J, Allaire PD, Legendre-Guillemain V, Zylbergold P, Gehring K, McPherson PS (2007). The NECAP PHear domain increases clathrin accessory protein binding potential. *EMBO J* 26, 4066–4077.
- Saffarian S, Kirchhausen T (2009). Distinct dynamics of endocytic clathrin coated pits and coated plaques. *Biophys J* 96, 569–570.
- Santini F, Marks MS, Keen JH (1998). Endocytic clathrin-coated pit formation is independent of receptor internalization signal levels. *Mol Biol Cell* 9, 1177–1194.
- Schmid SL, Frolov VA (2011). Dynamin: functional design of a membrane fission catalyst. *Annu Rev Cell Dev Biol* 27, 1–27.
- Segredo V, Burford NT, Lameh J, Sadee W (1997). A constitutively internalizing and recycling mutant of the mu-opioid receptor. *J Neurochem* 68, 2395–2404.
- Shenoy SK, Barak LS, Xiao K, Ahn S, Berthouze M, Shukla AK, Luttrell LM, Lefkowitz RJ (2007). Ubiquitination of beta-arrestin links seven-transmembrane receptor endocytosis and ERK activation. *J Biol Chem* 282, 29549–29562.
- Shin N, Ahn N, Chang-Ileto B, Park J, Takei K, Ahn SG, Kim SA, Di Paolo G, Chang S (2008). SNX9 regulates tubular invagination of the plasma membrane through interaction with actin cytoskeleton and dynamin 2. *J Cell Sci* 121, 1252–1263.
- Sorkin A, von Zastrow M (2009). Endocytosis and signalling: intertwining molecular networks. *Nat Rev Mol Cell Biol* 10, 609–622.
- Tanowitz M, von Zastrow M (2003). A novel endocytic recycling signal that distinguishes the membrane trafficking of naturally occurring opioid receptors. *J Biol Chem* 278, 45978–45986.
- Taylor MJ, Lampe M, Merrifield CJ (2012). A feedback loop between dynamin and actin recruitment during clathrin-mediated endocytosis. *PLoS Biol* 10, e1001302.
- Taylor MJ, Perrais D, Merrifield CJ (2011). A high precision survey of the molecular dynamics of mammalian clathrin-mediated endocytosis. *PLoS Biol* 9, e1000604.
- Terrillon S, Barberis C, Bouvier M (2004). Heterodimerization of V1a and V2 vasopressin receptors determines the interaction with beta-arrestin and their trafficking patterns. *Proc Natl Acad Sci USA* 101, 1548–1553.
- Tosoni D, Puri C, Confalonieri S, Salcini AE, De Camilli P, Tacchetti C, Di Fiore PP (2005). TTP specifically regulates the internalization of the transferrin receptor. *Cell* 123, 875–888.
- von Kleist *et al.* (2011). Role of the clathrin terminal domain in regulating coated pit dynamics revealed by small molecule inhibition. *Cell* 146, 471–484.
- Wolfe BL, Trejo J (2007). Clathrin-dependent mechanisms of G protein-coupled receptor endocytosis. *Traffic* 8, 462–470.
- Yu YJ, Dhavan R, Chevalier MW, Yudowski GA, von Zastrow M (2010). Rapid delivery of internalized signaling receptors to the somatodendritic surface by sequence-specific local insertion. *J Neurosci* 30, 11703–11714.
- Yudowski GA, Puthenveedu MA, Henry AG, von Zastrow M (2009). Cargo-mediated regulation of a rapid Rab4-dependent recycling pathway. *Mol Biol Cell* 20, 2774–2784.
- Zhang B, Koh YH, Beckstead RB, Budnik V, Ganetzky B, Bellen HJ (1998). Synaptic vesicle size and number are regulated by a clathrin adaptor protein required for endocytosis. *Neuron* 21, 1465–1475.